Application of first-pass contrast bolus tracking sequence for the assessment of morphology and flow dynamics in cardiac MRI

Yahya Paksoy, Orhan Özbek, Serter Gümüş, Osman Koç, Alaaddin Nayman, Ülkü Kerimoğlu

PURPOSE
There are two well-known indications for first-pass perfusion in the literature. First is the evaluation of myocardial ischemia, and the other is the evaluation of tumor vascularity. Our aim was to assess the value of a first-pass contrast bolus tracking sequence (FPCBTS) for cases unrelated to these pathologies.

MATERIALS AND METHODS
A total of 35 patients (age range, 1 day to 66 years; mean age, 10.4±19.2 years; median age, 4.5 months) with suspected congenital (n=31) and acquired (n=4) heart and great vessel disease were included in the study. All the patients underwent cardiac magnetic resonance imaging (MRI) and FPCBTS, and 20 patients underwent contrast enhanced magnetic resonance angiography (CE-MRA). We used cardiac MRI and CE-MRA for anatomic evaluation and FPCBTS for dynamic flow evaluation.

RESULTS
Truncus arteriosus, double outlet right ventricle, tetralogy of Fallot, corrected transposition of great arteries, atrial and ventricular septal defect, aortic rupture, cardiac hydatid cyst, tricuspid atresia, anomalous pulmonary venous return, and interrupted aorta were detected using the technique described here. Septal defects in six patients and atrial aneurysm in two patients were excluded. The shunt gap and flow direction of the septal defects, a ruptured wall in a dissected aorta, a hydatid cyst, and the atrial relationship in two cases with paracardiac masses were diagnosed easily using this dynamic evaluation technique.

CONCLUSION
FPCBTS can be performed in addition to cardiac MRI and CE-MRA to reveal flow dynamics and morphology.

From the Department of Radiology (Y.P.), Selçuk University Selçuklu School of Medicine, Konya, Turkey; the Department of Radiology (O.Ö., O.K., A.N., Ü.K.), Necmettin Erbakan University Meram School of Medicine, Konya, Turkey; the Department of Radiology (S.G. ✉ sertergum@yahoo.com), University of Pittsburgh, Pittsburgh, Pennsylvania, USA.

Assessment of the cardiac and great vessel anatomy is important in children and infants with congenital heart disease. Diagnosis of congenital pulmonary and great vessel anomalies helps clinicians to determine the appropriate management strategy for the patient. In the preoperative period, evaluation of the anomalous vascular anatomy guides the surgeon during the planning of the operation.

Echocardiography has been used as the primary diagnostic modality for the evaluation of congenital heart disease. However, this technique has limitations regarding the visualization of the pulmonary and great vessels and their connection sites (1). Catheter angiography is the gold standard imaging method for the evaluation of congenital vascular disorders, but it is a challenging, invasive procedure, and it includes ionizing radiation (1). Contrast enhanced magnetic resonance angiography (CE-MRA) has been successfully used to evaluate congenital vascular anomalies. With technical modifications, this technique can be performed during free breathing in infants and children. However, CE-MRA does not provide hemodynamic information as do catheter angiography and time-resolved MRA.

There are two well-known indications for first-pass perfusion in the literature. First is the evaluation of myocardial ischemia and the other is the evaluation of tumor vascularity. Our aim was to assess the value of a first-pass contrast bolus tracking sequence (FPCBTS) in cases that are unrelated to these pathologies.

Materials and methods

Between August 2006 and April 2008, 35 patients aged between 1 day and 66 years (mean age, 10.4±19.2 years; median age, 4.5 months) with suspected congenital heart or great vessel anomaly (n=31) and suspected acquired cardiac and great vessel pathology (n=4) were included in our study. All of the patients underwent cardiac magnetic resonance imaging (MRI) and dynamic FPCBTS examination as well as echocardiography. We performed CE-MRA in patients suspected of having great vessel pathology. In 20 patients, three-dimensional (3D) CE-MRA was performed as the first preoperative vascular imaging modality. Only three patients underwent catheter angiography as a complementary examination to 3D CE-MRA because the latter technique was not established as the gold standard procedure. Informed consent was obtained from all of the adult patients or from the parents of the children who underwent both MRI examination and catheter angiography. MRI was performed using a 1.5 Tesla system (Magnetom Symphony, Siemens, Erlangen, Germany) equipped with a high-performance three-axis gradient system. For signal detection, the combination of a six-channel body phased-array coil and a two-channel spine phased-array coil was used in adults and large children. A head or extremity coil was used in infants and small children.

In the cardiac MRI protocol, an ECG-gated, dark blood, half-Fourier, single shot, fast spin echo sequence (HASTE) (TR, 770; TE, 35 ms; section thickness, 3–5 mm; matrix, 192×256) was performed in the axial and coronal planes for localization. Then, two- and four-chamber and short-axis steady-state cine were acquired in free precession (SSFP or FISP) images (TR, 63; TE, 1.92 ms; section thickness, 46 mm; matrix, 192×256).

In our FPCBTS imaging protocol, four slices of a single-shot turbo FLASH sequence with saturation recovery preparation (TR/TE, 298/1.66 ms; inversion time, 200 ms; flip angle, 12°; temporal resolution, 1.5 s; matrix, 96×128; slice thickness, 6–8 mm) displaying the optimal view of the related pathology were chosen from the cine and black blood studies. For each slice, 20–40 consecutive images were acquired. In most of the patients, a dynamic evaluation was performed before 3D CE-MRA. However, in four patients we had to perform the dynamic evaluation after CE-MRA. We attempted to evaluate the complex congenital pathologies while each patient was in the examination room. In four cases, we decided to use FPCBTS after evaluating MRA images. Therefore, we had to wait at least 15 min for the clearance of the contrast material from the blood flow. During this time, other sequences for cardiac MRI were acquired.

We used 0.1 mL/kg of the contrast agent for FPCBTS. The contrast material was administered intravenously followed by 3-20 mL saline solution. This combined approach was helpful for assessing both the vascular anatomy and the flow hemodynamics of the patients. A 3D CE-MRA was performed in the coronal plane using following sequence parameters: TR, 4.66 ms; TE, 1.78 ms; flip angle, 35°; slab thickness, 70–90 mm; effective thickness, 1.5 mm with elliptic centric reordering k-space coverage; bandwidth, 390 Hz/pixel, and a total duration of 8–12 s for each phase. A 3D CE-MRA was performed after injection of gadolinium chelate (Magnevist, Schering, Berlin, Germany and Omniscan, Amersham-Health, Oslo, Norway) through the antecubital vein at a cumulative dosage of 0.2 mmol/kg (total dosage with FPBTS) injected by hand followed by a rapid flush with 5–20 mL of normal saline, and the imaging sequence was begun with the care bolus sequence. After contrast injection, three consecutive data sets were acquired. Postcontrast scans were obtained with the same parameters as the precontrast scans, and the postcontrast dataset was subtracted from the precontrast dataset. Postprocessing of the subtracted raw data was performed on a workstation (Leonardo, Siemens Medical Systems, Erlangen, Germany). A 3D multiprojection volume reconstruction was performed. A targeted maximum intensity projection was obtained. Catheter angiography was performed by a pediatric cardiologist.

Results

In total, 35 patients were examined. Of these patients, six had normal cardiac anatomy. Of these six patients, one had persistent left superior vena cava (Figs. 1, 2). The distribution of the remaining patients was as follows: truncus arteriosus (n=7), double outlet right ventricule (n=4), tetralogy of Fallot (n=2), corrected transposition of the great vessels (n=2), atrial septal defect (n=3), isolated ventricular septal defect (n=1), aortic rupture (n=1), cardiac hydatid cyst (n=1), tricuspid atresia (n=2), anomalous pulmonary venous return (n=2), paracardiac mass (n=2), and interrupted aorta (n=2). Other related secondary and tertiary anomalies were summarized in Table.

In patients with atrial septal defect or ventricular septal defect, when the contrast arrived at the right chambers, it was much easier to detect shunting from right to left because the left chambers were empty (Fig. 3). When left-to-right shunting was the concern, shunting was observed as a negative flow through the contrast medium in the right chambers space. The contrast in the right chambers has to be washed out before it arrives in the left chambers, and this state was achieved by decreasing the amount of contrast medium with a fast injection and subsequent physiologic flush serum. In patients with atrial septal defect, both right-to-left and left-to-right shunting were present (Fig. 4).

In both isolated ventricular septal defect and in ventricular septal defect accompanying a primary pathology, right-to-left shunting was present, and the shunting could also be demonstrated through the dynamic analysis (Fig. 3).

In cases with truncus arteriosus, because of the overlying position of the aorta, contrast arrival at the aorta occurred before the arrival of contrast at the left atrium and pulmonary veins. Depending on the type of truncus, enhancement of the pulmonary artery occurred with or after the enhancement of the aorta. Especially in cases with type-1 truncus, pulmonary artery enhancement occurred simultaneously with enhancement of the aorta, but in patent ductus arteriosus or in cases involving multiple aortapulmonary collateral arteries, pulmonary artery was enhanced after the aorta. Pulmonary vein enhancement occurred after enhancement of the aorta in all truncus cases (Fig. 5).

In two cases with the supracardiac type anomalous pulmonary venous return, contrast material crossed from the right atrium to the left atrium via the atrial septal defect and to the aorta by the left ventricle. The left ventricle and left atrium were enhanced prior to the pulmonary veins. The pulmonary veins were opened into a pouch that was drained into the superior vena cava via the vertical vein. Enhancement of the pouch prior to the left atrium was easily demonstrated in dynamic FPCBTS images (Fig. 6).

In two cases with tricuspid atresia, while the left atrium and ventricle were being filled with contrast medium via the atrial septal defect, the hypoplastic right ventricle was filled via the ventricular septal defect. In two cases of tetralogy of Fallot, due to overlying position of the aorta, contrast arrival at the aorta occurred prior to arrival at the left ventricle because the right ventricle was pumping contrast medium to the aorta and pulmonary artery simultaneously (Fig. 3).

In one patient with a ruptured ascending aortic aneurysm, the ruptured wall and the contrast filling of pseudolumen were demonstrated dynamically. This analysis showed that the pseudolumen was not thrombosed. The rupture was limited, and there was no leakage (Fig. 7).

In a case with a hydatid cyst, black blood and SSFP (FISP) images showed a mass lesion whose borders were not clearly differentiated from myocardium because of the degenerated pattern of the cyst (i.e., solidification of cyst). Dynamic analysis showed that the lesion was avascular and had a
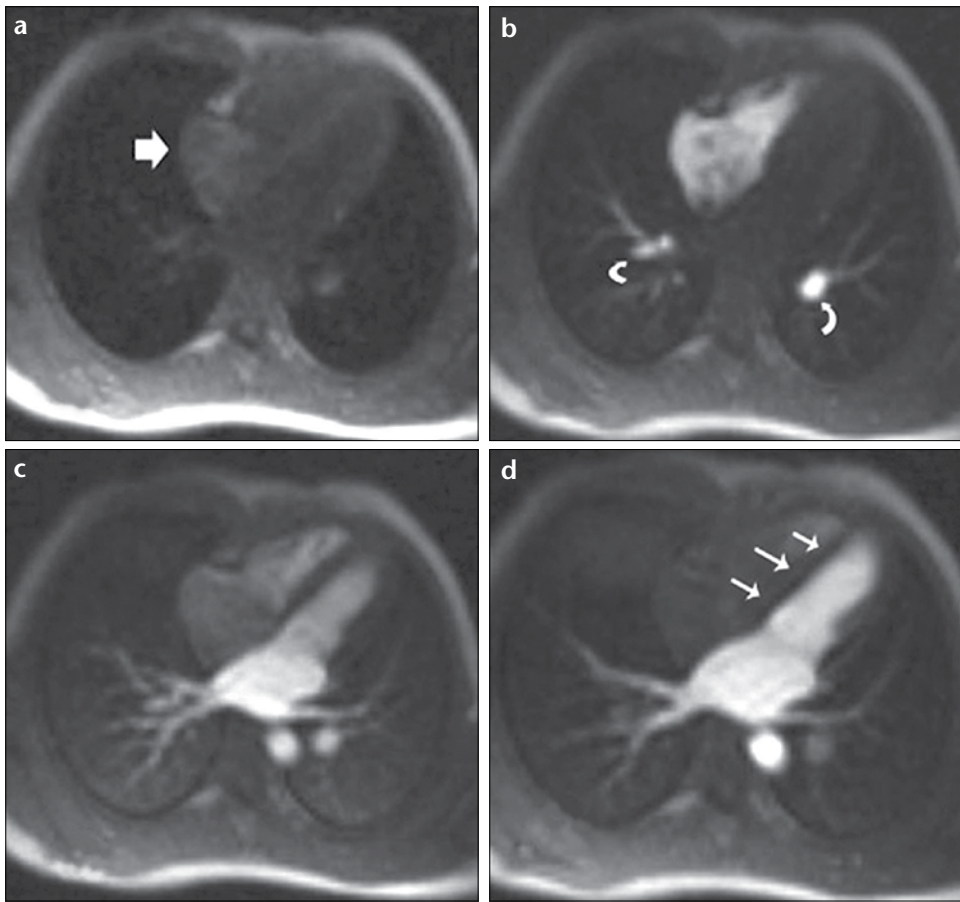
Figure 1. a–d. Normal anatomy on cardiac MRI. Intravenously administered contrast medium first arrives at the right atrium (**a**, *thick arrow*). As the contrast medium fills the right ventricle, enhancement of the pulmonary arteries begins (**b**, *curved arrows*). The pulmonary veins, left atrium, and left ventricle are enhanced. The aorta becomes enhanced at the same time as the contrast agent fills the pulmonary veins, the left atrium, and the left ventricle (**c**). The beginning of the right atrial contrast medium wash-out can also be depicted. The contrast material was cleared from the right heart chambers (**d**). The enhancement of the right chambers of the heart occurs at the same time as the enhancement of the pulmonary arteries. The contrast filling of the left heart chambers occurs at the same time as the aorta. There is no septal defect (**d**, *thin arrows*).
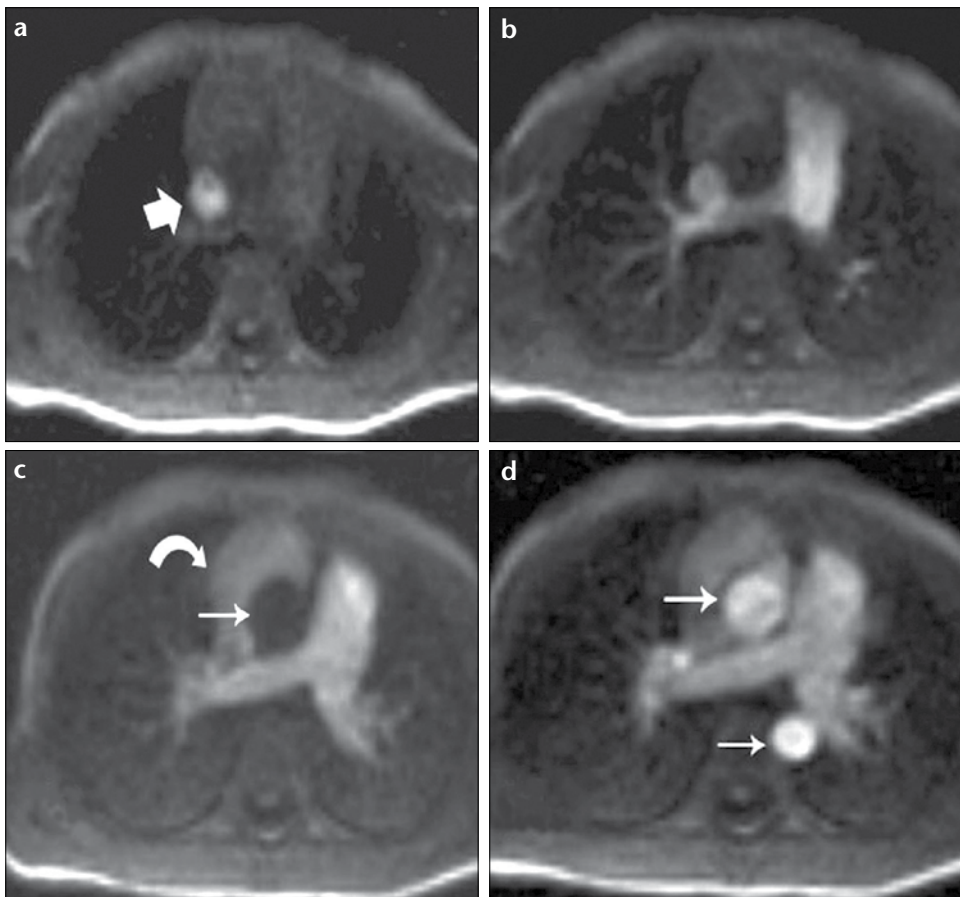

Figure 2. a–d. Normal anatomy on cardiac MRI. Image series obtained from an upper level. Intravenously administered contrast medium first arrives at the superior vena cava (**a**, *thick arrow*). Other great vessels are still empty. Then, pulmonary artery enhancement occurs (**b**). The aorta is still empty (**c**, *thin arrow*). The contrast filling of the right atrial appendix can also be depicted (**c**, *curved arrow*). Ascending and descending aorta contrast filling can be observed in the last phase (**d**, *arrows*).

Table. Demographic data of the study patients

Primary pathology	Number of patients	Age	Additional pathology	FPCBTS findings	MRA findings	SSFP findings
Atrial septal defect	3	1 day 2 days 2 days		Right to left shunting	Not performed	Atrial septal defect
Tricuspid atresia	1	1 day	Atrial septal defect, pulmonary atresia, patent ductus arteriosus	Filling of contrast medium to left ventricle before right ventricle and filling of aorta before pulmonary artery and vein	Patent ductus arteriosus, patency and truncus and pulmonary artery connection	Atrial septal defect
Tricuspid atresia	1	10 months	Ventricular septal defect, atrial septal defect	Right ventricle is being filled with contrast from left ventricle via ventricular septal defect.	Truncus and pulmonary arter connection	Atrial and ventricular septal defects
Ventricular septal defect	1	5 days	Hypoplastic aortic arcus, atrial septal defect, ventricular septal defect, patent ductus arteriosus	Right to left shunting via ventricular septal defect. Left ventricle was filling before the filling of pulmonary vein with contrast medium.	Hypoplastic aortic arch and patent ductus arteriosus	Atrial and ventricular septal defects
Tetralogy of Fallot	2	4 years 2 months	Related pathologies	Filling of aorta occurs before left ventricle due to overriding aorta.	Overriding aorta and pulmonary stenosis and hypoplasia	Overriding aorta, atrial and ventricular septal defects
Transposition of the great arteries	2	8 years 56 years	Atrial septal defect, dextro position of aorta, left persistant superior vena cava	Contrast material directly goes to morphologic right atrium and left ventricle.	Position of great vessels	Position of cardiac chambers and morphology
Truncus (Type 4)	3	1 year 3 days 1 day	Related pathologies	After right-sided injection, filling of aorta occurs before left atrium. Pulmonary artery filling occurs after aorta.	Truncus and related pulmonary connections	Ventricular and atrial anatomy
Truncus (other types)	4	2 months 1 day 5 days 3 days	Related pathologies	Filling of aorta and pulmonary artery occurs at the same phase.	Truncus and related pulmonary connections	Ventricular and atrial anatomy
Aortic rupture	1	58 years		Rupture site and filling of aneurysm		
Hydatid cyst	1	36 years		The mass lesion which can not be distinguished from myocardium on FLASH and black-blood series showed no contrast enhancement in dynamic evaluation.	Not performed	Mass
Prediagnosis of atrial aneurysm	2	66 years 55 years		Patient suspected of having atrial aneurysm demonstrates no enhancement in atrial phase, but enhancement with aorta.	Not performed	Mass
Suspicion of atrial or vetricular septal defect	6	4 years 2 years 18 years 5 years 7 years 5 years	Persistant left vena cava in one case	Normal findings	Not performed	Ventricular and atrial anatomy
DORV	3	11 years 1 month 1 month	Hypoplastic left ventricle, azigos continuity, situs inversus totalis, no inferior vena cava (in one case)	Filling of aorta occurs before pulmonary veins. Contrast filling to aorta is seen before left heart chambers.	DORV and absence of inferior vena cava (one case)	Ventricular and atrial anatomy
DORV	1	2 months	Persistant left vena cava, unroof coronary sinus	Filling of aorta occurs before pulmonary veins in right arm injection. Contrast filling to aorta is seen before left heart chambers. Left arm injection showed left atrial and left ventricular enhancement before than right chambers because of unroof coronary sinus and left persistant vana cava.	Not performed	Ventricular and atrial anatomy
Interrupted aorta	2	1 day 1 day	Patent ductus arteriosus	Filling of thoracic aorta occurs before left ventricle.	Aortic interruption and patent ductus arteriosus	Ventricular and atrial anatomy
APVR	2	4 months 5 months	Atrial septal defect	Right to left shunting: atrial septal defect. Left ventricle and left atrium were being enhanced prior to pulmonary veins. Pulmonary veins were opening to a pouch which was being drained to superior vena cava via vertical vein. Enhancement of the pouch prior to left atrium was easily demonstrated in dynamic analysis.	APVR	Ventricular and atrial anatomy

APVR, anomalous pulmonary venous return; DORV, double outlet right ventricle; FPCBTS, first-pass contrast bolus tracking sequence; MRA, magnetic resonance angiography; SSFP, steady-state free precession.
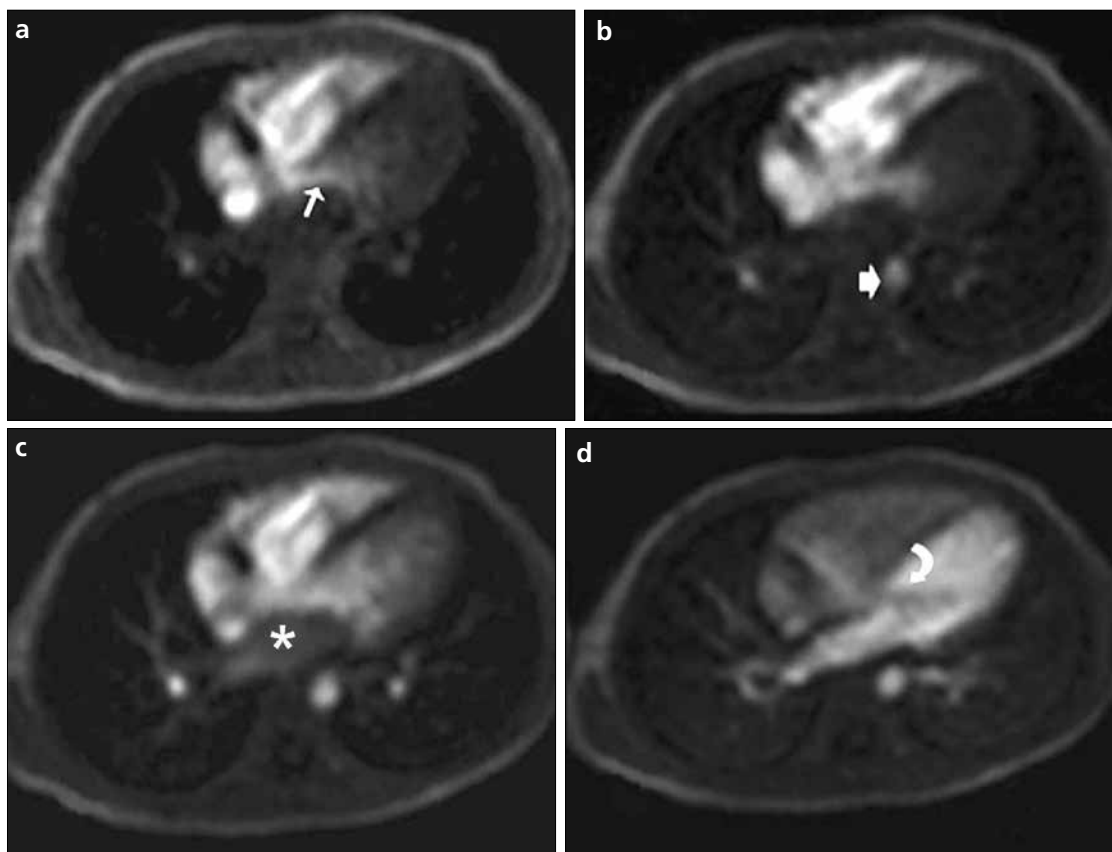
Figure 3. a–d. Cardiac MR images of the ventricular septal defect and right-to-left shunt *(thin arrow)* in a patient with tetralogy of Fallot **(a)**. The aorta, the left atrium, and most of the left ventricle are still unenhanced. In this phase **(b)**, while much of left ventricle is still empty due to the overlying position of the aorta, arrival of the contrast agent at the aorta *(thick arrow)* occurs prior to filling of the left ventricle and left atrium. Left ventricle enhancement proceeds **(c)**. The left atrium is still empty **(c,** *asterisk***)**. Contrast filling of the pulmonary veins and left atrium occurs in the last phase **(d)**. Because the right side of the heart is washed out in this phase, the shunting flow via ventricular septal defect forms a negative flow effect in the left ventricle **(d,** *curved arrow***)**.
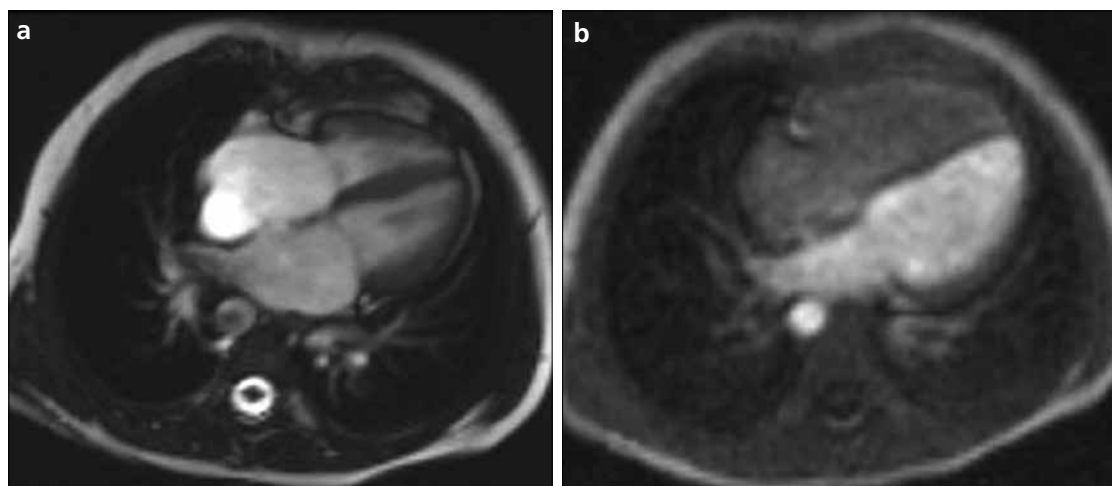

Figure 4. a, b. Left-to-right shunting via atrial septal defect in FISP **(a)** and FPCBTS **(b)**.

similar enhancement pattern as another lung lesion observed in the same slice. These features facilitated the diagnosis of the lesion observed in myocardium (Fig. 8).

In two cases with paracardiac masses neighboring the atrium that had previously been suspected as atrial aneurysms, dynamic analysis demonstrated that the lesions were not connected to the atrium and were enhanced in the arterial phase as solid lesions. In two cases with corrected type of transposition of great arteries (atrioventricular and ventriculoarterial discordance),
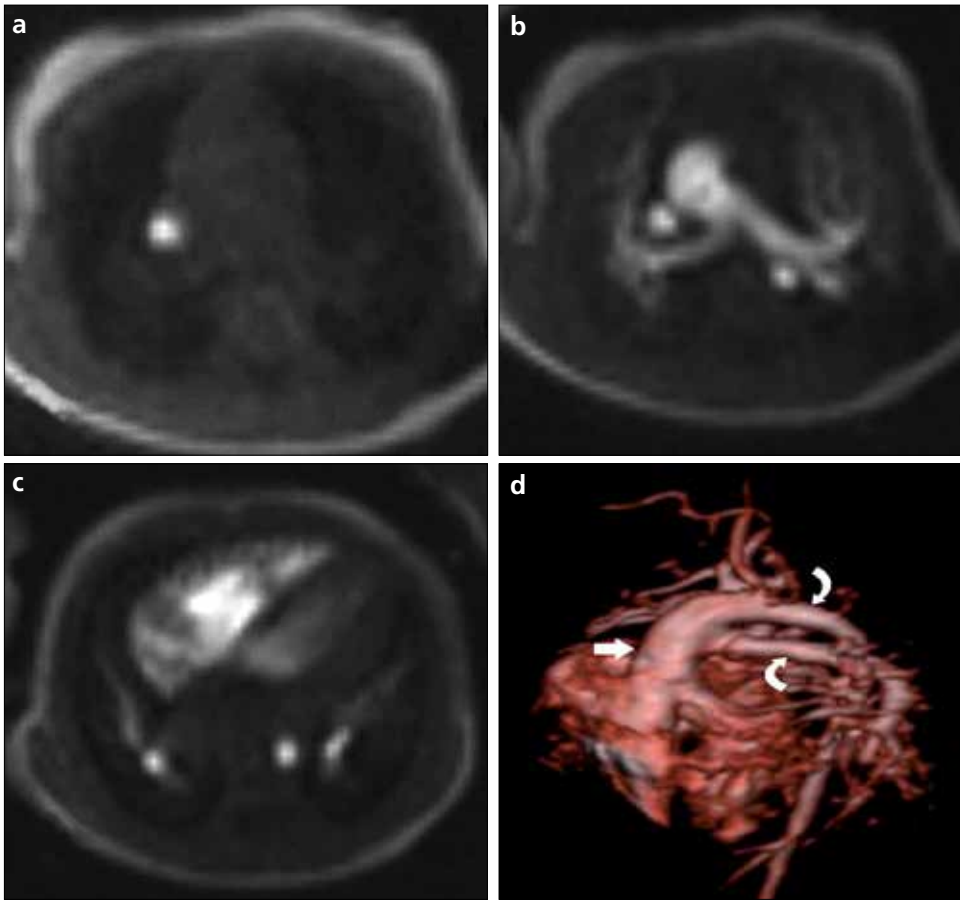
Figure 5. a–d. A patient with truncus arteriosus type-1. On cardiac MRI, intravenously administered contrast medium first arrives at the superior vena cava (a). The main truncus and main pulmonary artery are enhanced at the same time (b). Pulmonary arterial branches directly originating from the main truncus can also be depicted. Shunting from the right to the left via ventricular septal defect is seen (c). The pulmonary artery and the main truncus are enhanced at the same time, before the enhancement of the pulmonary veins and left atrium. The origin of the pulmonary artery (curved arrows) at the main truncus (thick arrow) can be depicted on a 3D volume rendering technique based on CE-MRA (d). The overlying position of the aorta can also be observed on close examination.
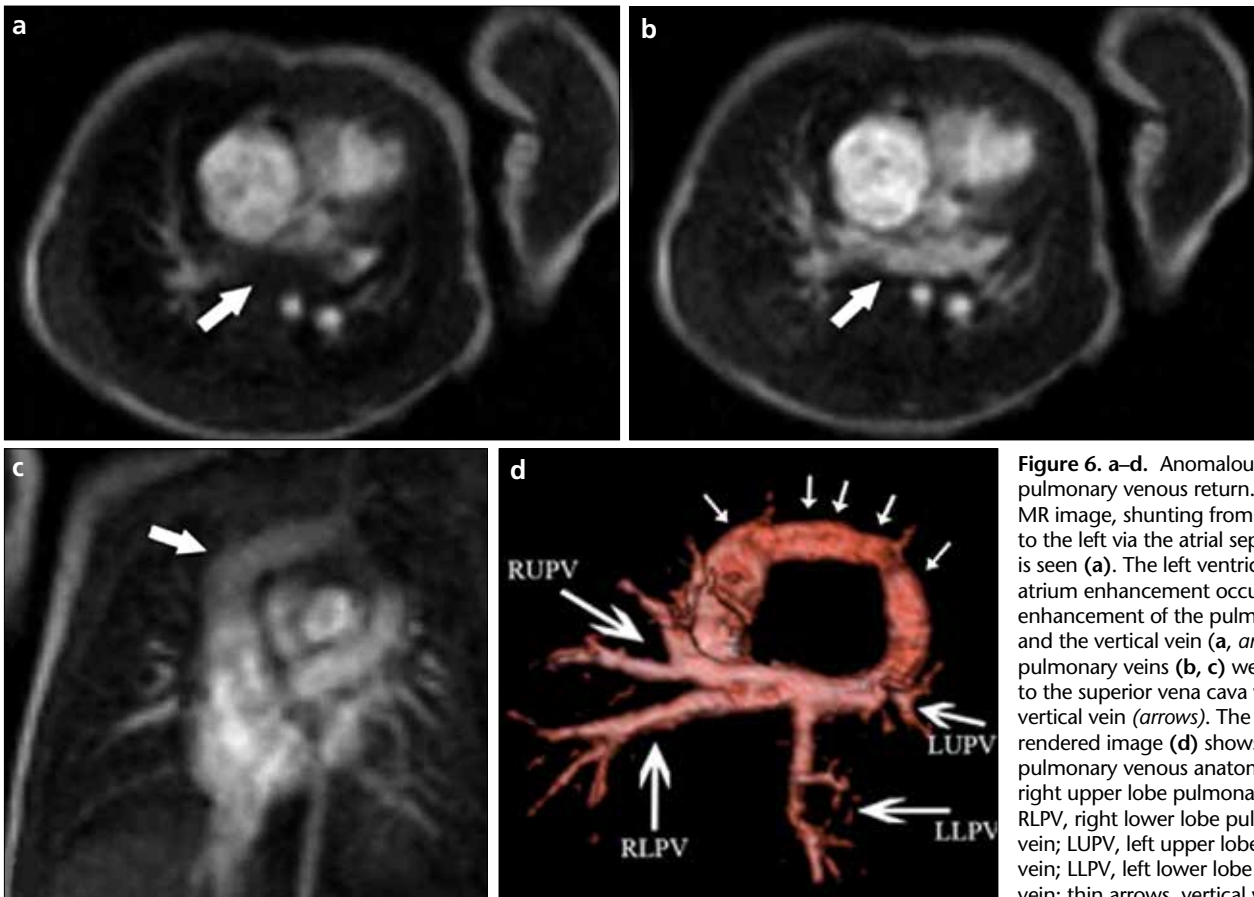

Figure 6. a–d. Anomalous pulmonary venous return. On cardiac MR image, shunting from the right to the left via the atrial septal defect is seen (a). The left ventricle and left atrium enhancement occurs prior to enhancement of the pulmonary veins and the vertical vein (a, arrow). The pulmonary veins (b, c) were drained to the superior vena cava via the vertical vein (arrows). The volume rendered image (d) shows the pulmonary venous anatomy. RUPV, right upper lobe pulmonary vein; RLPV, right lower lobe pulmonary vein; LUPV, left upper lobe pulmonary vein; LLPV, left lower lobe pulmonary vein; thin arrows, vertical vein.
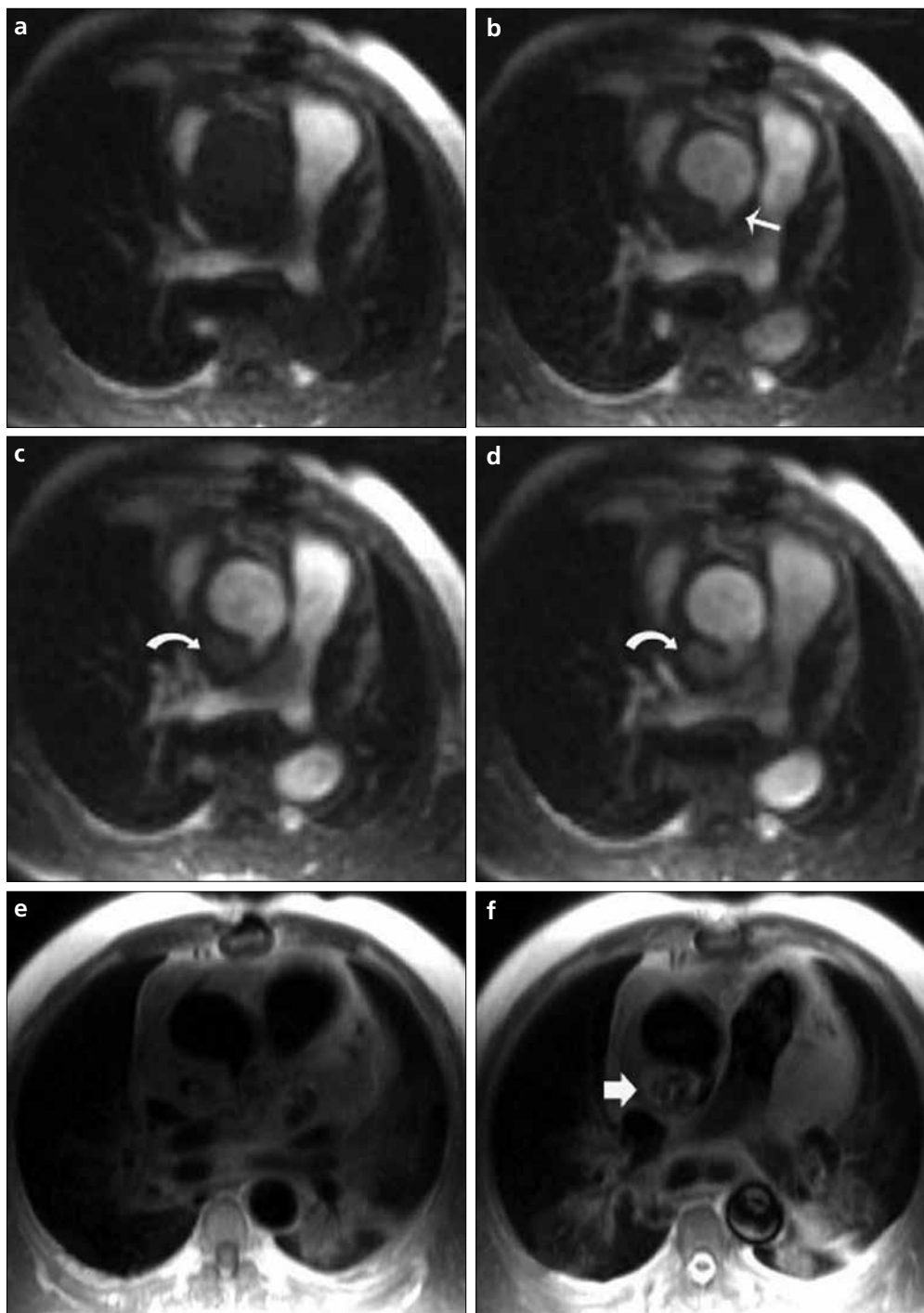
Figure 7. a–f. The filling of pseudoaneurysm over time in a patient with a ruptured aorta. The pulmonary artery fills with contrast first while the aorta is still empty **(a)**. The aorta begins to be enhanced **(b)**. In this phase, only the ruptured wall *(thin arrow)* can be seen. Contrast filling of the pseudolumen **(c, d)** proceeds *(curved arrows)*. The patency of the pseudolumen cannot be clearly differentiated in the black blood series **(e, f)**, and there is an impression of a thrombosis *(thick arrow)*.

the injected contrast material was delivered directly to the morphologic right atrium and left ventricle. In both cases, accompanying abdominal situs inversus, persistent left superior vena cava, and dextroposition of the aorta were present (Fig. 9).

In four cases with double outlet right ventricle, contrast filling of the aorta occurred prior to filling of the pulmonary veins and/or the left chambers of heart. In one of these cases, accompanying a hypoplastic left ventricle, azygos continuity, situs inversus totalis, and agenesis of the inferior vena cava were present. One of the other cases had a persistent left superior vena cava and an unroofed coronary sinus. Injection into the left arm showed left atrial and left ventricular enhancement before enhancement of the right chambers because of an unroofed coronary sinus and a left persistent vena cava (Figs. 10, 11). Injection into the right arm showed the prior right atrium enhancement in this case.

Discussion

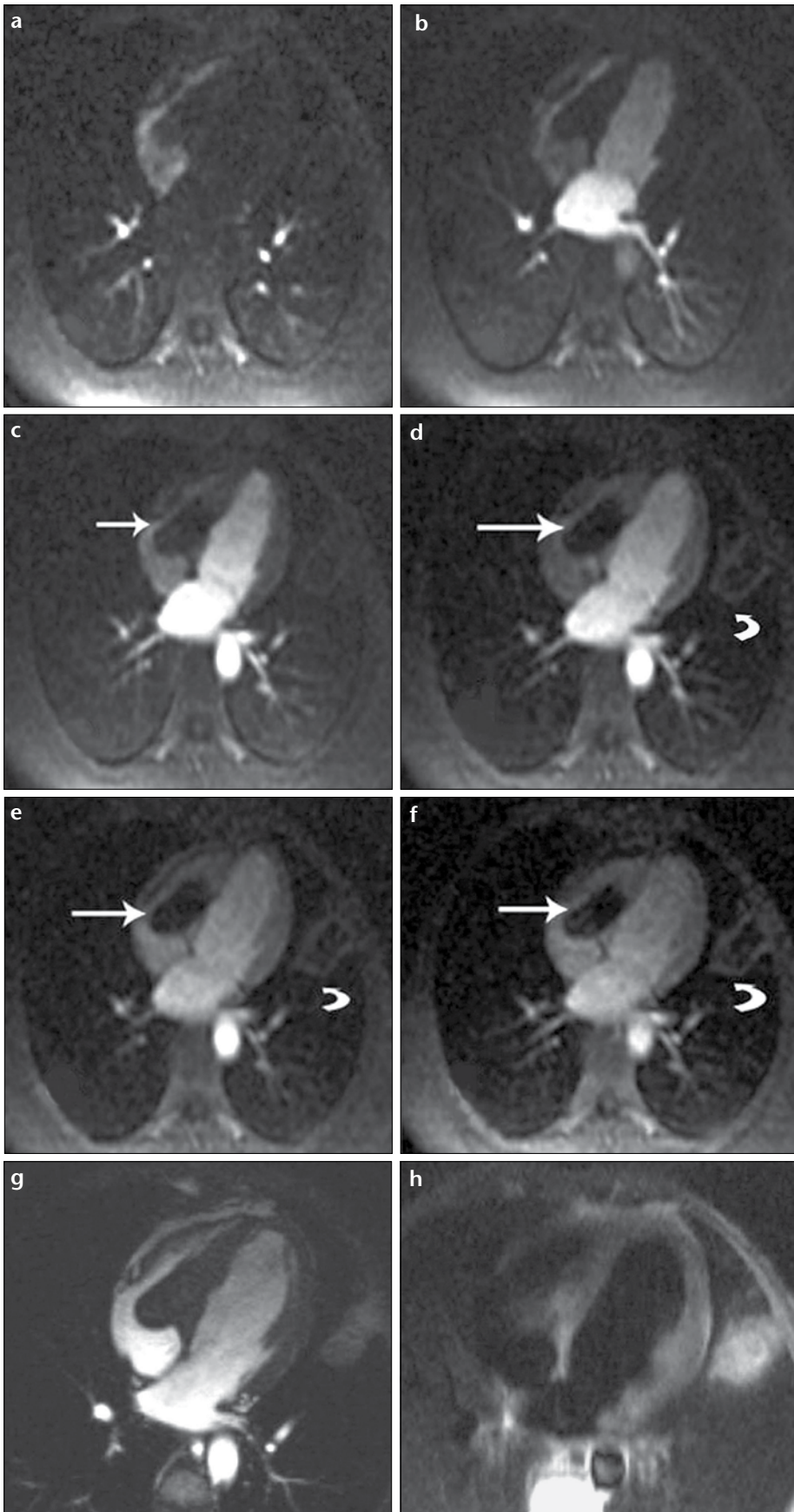Accurate assessment of cardiovascular circulation is important for many

Figure 8. a–h. Because the heart chambers and myocardium become enhanced after contrast administration, a nonenhanced, degenerated hydatid cyst can clearly be depicted because of its avascular nature (**a–f**, *arrows*). A similar lesion in the left lung shows the same contrast enhancement pattern *(curved arrows)*. The hydatid cyst cannot be differentiated from the myocardium of the interventricular septum in SSFP images **(g, h)** It is much easier to differentiate it on FPCBTS **(a–f).**
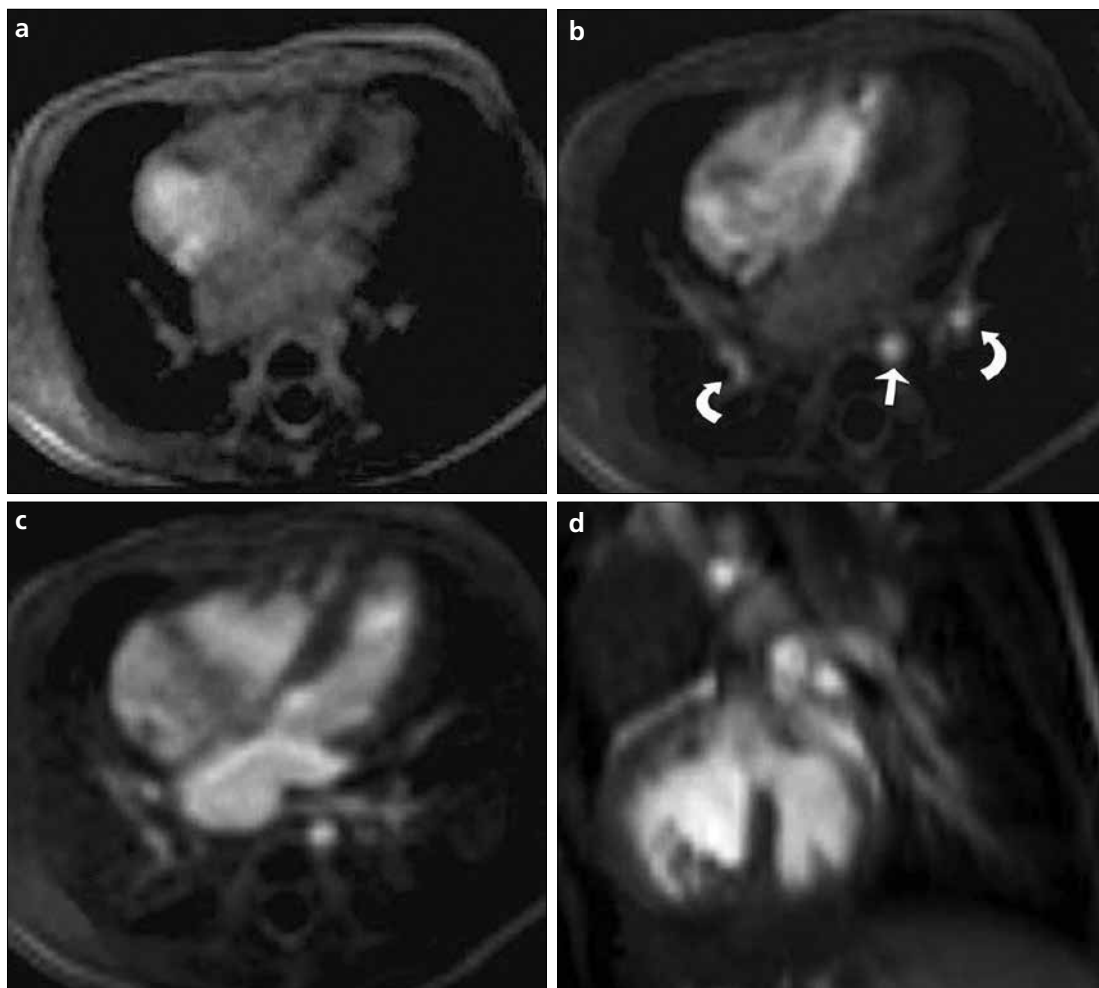
Figure 9. a–d. Double outlet right ventricle on cardiac MRI. Contrast enhancement of the aorta *(arrow)* and pulmonary artery *(curved arrows)* occurs at the same time **(a, b)**, just after contrast filling of the right ventricle. At this time; the left ventricle, left atrium, and pulmonary veins are still empty. In the next phase the left ventricle **(c)**, left atrium, and pulmonary veins **(d)** enhance. In the SSFP image, the double outlet right ventricle can be clearly depicted.

cardiopulmonary disorders, especially complex congenital heart diseases that involve complicated interactions between the systemic and pulmonary circulation (2, 3). Catheter-based angiography with pressure measurements is the standard method for obtaining anatomical and functional information about the vessels of interest. However, this method is invasive and difficult to perform, especially in newborns, and it exposes patients to ionizing radiation (4). MRA has been used to evaluate congenital cardiovascular heart disease. MRA has certain benefits and advantages compared to catheter angiography. The sedation time is reduced in the MRA procedure. CE-MRA does not require expertise to be performed on small children, and there is no need for arterial puncture. MRA is performed without use of ionizing

radiation, and only a small amount of contrast agent is used, having no known nephrotoxicity and revealing a low frequency of allergic reactions (1). If there is any existing renal failure, one must avoid any complication of the nephrogenic systemic fibrosis. In our patient population, none of the subjects had renal failure of any grade. We also used only a small amount of contrast medium for the first-pass imaging. There are reported complications of arterial catheterization in children; the incidence is low but not negligible (5). Diagnosis before surgery is required to prevent unnecessary and incorrect surgical procedures. Thus, we aimed to investigate the feasibility of using cardiac MRI noninvasively to visualize cardiovascular anomalies and hemodynamic flow using a contrast agent and an MR scanner, which

presents no radiation risk, instead of conventional angiography. Although 3D CE-MRA has been proposed as an alternative technique to conventional angiography for evaluating the vascular anatomy (6–8), it provides limited information about hemodynamics for bolus tracking. Therefore, it is clinically important to develop a noninvasive method that can reveal anatomic details, enable bolus chasing in the cardiopulmonary circulation, and be generally applicable to pediatric patients. Dynamic FPCBTS has a temporal resolution of approximately 1.5 s per frame, and it has been shown to simultaneously depict the major elements of cardiopulmonary circulation. To our knowledge, however, FPCBTS has not been applied to the evaluation of complex cardiovascular circulation patterns associated with congenital
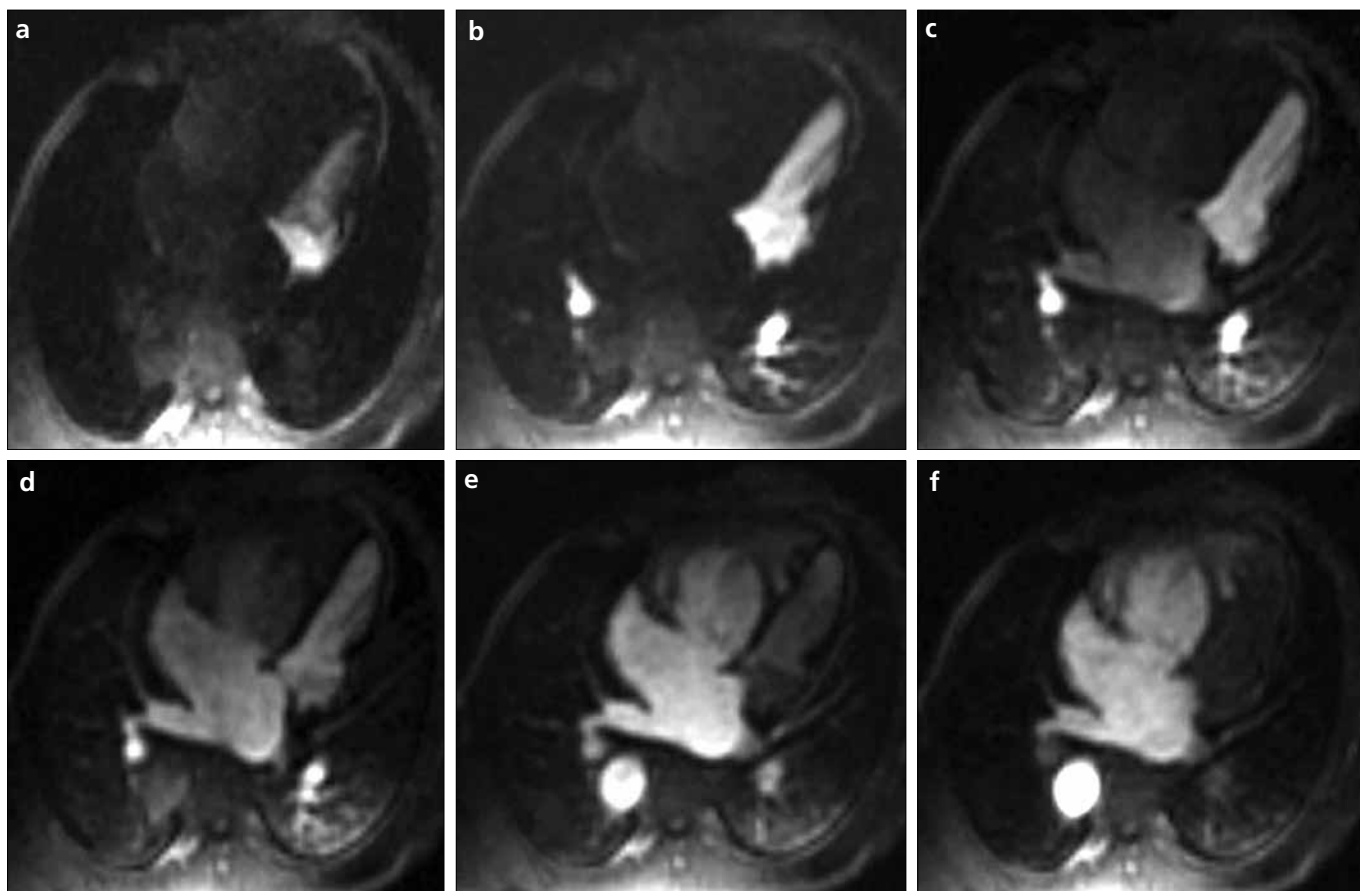
Figure 10. Cardiac MR images of the corrected type transposition of the great arteries. The left chambers of the heart are filled first, and then the left ventricle pumps the blood to the pulmonary artery and the right ventricle pumps it to the aorta.

heart disease. Performing FPCBTS together with CE-MRA may represent a new application for the evaluation of flow dynamics in a wide spectrum of cardiac and vascular diseases. In this respect, we hypothesized that FPCBTS could help to visualize the direction of blood flow, and thereby facilitate the evaluation of flow dynamics and the pulmonary and systemic circulation in such patients.

CE-MRA provides diagnostic images within less than one minute after injection of the contrast material into a peripheral vein (1, 9–11). Disadvantages of the MRA have been reported, including inadequate spatial resolution in small children to evaluate pulmonary vascular anomalies, and inadequate temporal resolution to reveal the time-resolved contrast passage in anomalous pulmonary circulation (1, 10, 12, 13). With the implementation of the new high performance gradient systems, both the spatial and the temporal resolution of the MRA have been improved (1, 14). In our dataset,

the apparent section thickness was set to 1.5 mm or less, revealing a sufficient spatial resolution to obtain detailed anatomical information about the pulmonary vasculature and avoid superposition of the pulmonary veins and arteries. With the use of targeted maximum intensity projection reconstructions, the suspected area on a volumetric dataset was evaluated in a thinner slab.

Cardiac and great vessel anomalies can be imaged in clinical practice with the use of black-blood MRI, CE-MRA, cine MRI, and phase-contrast (PC)-MRI. Furthermore, detailed flow dynamics according to the geometric characters of the cavopulmonary connections have been investigated by means of more sophisticated MRI techniques, such as 3D PC imaging (9) and cine imaging with a presaturation pulse (15–17). Due to recent advances in MRI techniques, including parallel imaging and undersampling of the k-space, time-resolved CE-MRA has become available on clinical scanners.

Clinical studies have demonstrated the usefulness of time-resolved CE-MRA (15, 18, 19). Of course time-resolved CE-MRA has the advantage of being 3D, but this technique is not widely available. In our method, we could perform different slice plans according to the suspected underlying pathology. On the other hand, the FPCBTS method is 2D, and it is different from the time-resolved CE-MRA. With a small amount of contrast material, one can obtain useful information about the blood flow dynamics.

Temporal resolution is important to evaluate abnormal cardiac circulation patterns. In our cases, anomalous cardiac circulation was identified with the use of the FPCBTS. The use of this recently developed, rapid imaging sequence in myocardial perfusion under conditions of pharmacologic stress during the first pass of contrast agent in myocardial tissue has been previously described (20). This new technique has been used in breath-holding sequences in adults. Breath-hold imaging
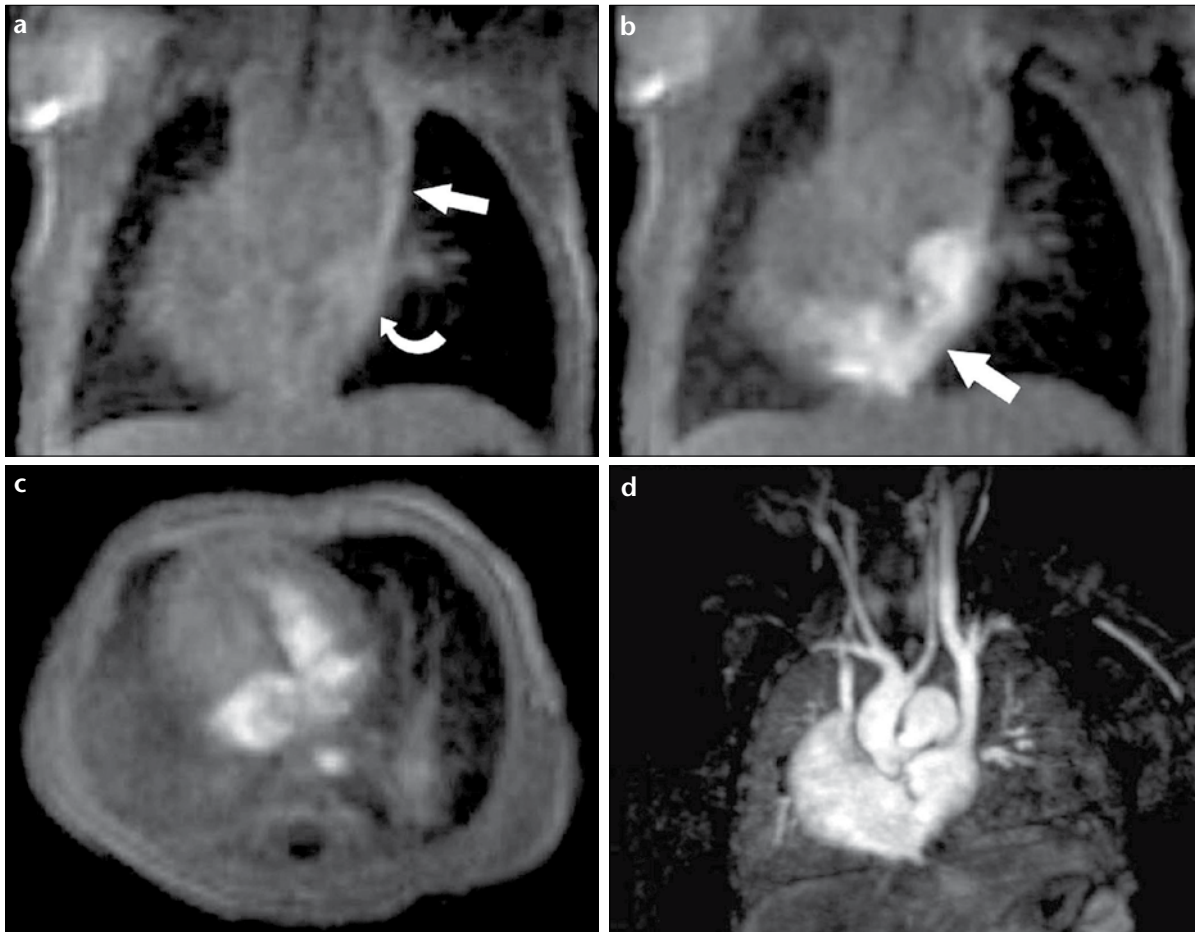
Figure 11. a–d. Left arm injection showing left atrial and left ventricular enhancement before the right chambers because of the unroofed coronary sinus and the left persistent vena cava. This patient had dextraposition as well. Contrast medium filling of the left persistent vena cava *(arrow)* and the left atrium *(curved arrow)* is seen **(a)**. FPCBTS **(b)** shows left-to-right shunting via the unroofed coronary sinus *(arrow)*. Axial FPCBTS **(c)** shows contrast medium filling of the left atrium, left ventricle, and aorta before right ventricle filling. Subvolumetric CE-MRA **(d)** shows the bilateral superior vena cava and their connections with the atria.

in sedated infants and children is not possible, and thus free breathing MRI was performed.

A double or triple dose of contrast agent can be used to improve the image quality on images that are susceptible to breathing artifacts. We used less than a triple dose of contrast agent in total if the patient had CE-MRA and FPCBTS. Subtraction of the contrast-enhanced images from the noncontrast scans enabled delineation of vascular structures.

In this pilot study, we were able to assess the flow dynamics of the heart and great vessels, as well as their morphology by FPCBTS with high temporal and adequate spatial resolution. Our study demonstrates the feasibility of visualizing the flow dynamics in congenital heart disease and other cardiac and paracardiac pathologies. Several MRI techniques have been

used to visualize congenital heart disease and cardiac pathologies, but until now, the diagnosis of flow direction and characterization of the hemodynamic pattern have not been possible using MRI because of insufficient spatial and temporal resolution and the absence of a dynamic evaluation. Catheter angiography is usually regarded as the sole imaging modality for evaluating the flow dynamics of cardiovascular structures. Based on our results and those of other investigators (18, 19), we believe that FPCBTS may be used for the dynamic evaluation in some cases because it can achieve both high spatial and temporal resolution. Therefore, in combination with other cardiac MRI techniques, such as cine imaging, PC imaging, and black-blood imaging, the use of 3D CE-MRA and FPCBTS can potentially extend the comprehensiveness of cardiac

MRI. Moreover, we were able to visualize first-pass circulation by FPCBTS using a low dose of gadolinium instead of the standard dose. The results presented in this study underline the potential of FPCBTS to detect hemodynamics noninvasively and reliably. However, our findings warrant further investigation.

In our study, abnormal cardiovascular circulation was correctly assessed using dynamic FPCBTS. Cardiovascular and paracardiac pathologies were diagnosed correctly using dynamic FPCBTS, and the results correlated well with the diagnoses of the catheter angiography, and the exact final diagnosis was established according to cardiac MRI, echocardiography, surgery, CE-MRA, or catheter angiography.

FPCBTS was successfully performed on all 30 patients with no examination-associated complications. The flow

dynamic was effectively determined by the FPCBTS, which had a temporal resolution of less than 2 s. The examination times did not exceed 30 min in 30 patients, except in four patients who underwent additional dynamic evaluation after CE-MRA. We had to wait an additional 15 min for clearance of the contrast medium from the heart, so the examination time was longer in those four patients. Although motion artifacts were noticeable in free-breathing studies, they were mild and did not restrict the ability to make a diagnosis.

To the best of our knowledge, the use of a small amount of gadolinium for first-pass imaging in patients who have cardiac, paracardiac, and great vessel pathologies has not been evaluated. As expected, FPCBTS was fairly resistant to motion artifacts, so respiratory motion artifacts resulting from free breathing were within the acceptable ranges.

There are several limitations of our study that should be addressed. Unfortunately, this sequence is acoustically very noisy, although no sedated patient was woken up during the examination. Other limitations of the present study are the small number of patients whose FPCBTS results were correlated with the results of catheter angiography. Fortunately we did not need to use this invasive technique in most of our pediatric patients. Thus, the transferability of our findings into a routine setting is limited. Further studies with larger patient populations to provide correlation with conventional angiography and echocardiography are needed to confirm these initial results. Compared with transesophageal echocardiography, contrast-enhanced MRI examinations currently are more expensive and require a longer examination time.

Another limitation of this study was that we used two times more of the recommended dose of the contrast agent for pediatric cases. None of our patients exhibited renal function abnormality, and none of them experienced acute or long-term complications. After introduction of nephrogenic systemic fibrosis, we believe that for MRA purposes, one should use the recommended doses.

Until now, blood circulation has not been diagnosable in real time by standard MRI-techniques except time resolved MRA. Spin echo as well as cine gradient echo and even SSFP do not allow for real-time detection of the entire pattern of blood circulation in a single step.

We believe that with the availability of fast imaging, our method can further enhance the clinical diagnostic utility of FPCBTS in patients with cardiac and great vessel anomalies. Temporal resolution is one of the most important features in this method. The image quality is much better in patients with low heart rates. Bolus chasing via FPCBTS analysis improved the diagnostic usefulness of CE-MRA and complemented anatomic imaging for evaluating cardiopulmonary circulation in pediatric patients with complex congenital heart disease.

As a conclusion, FPCBTS, which is used traditionally in myocardial perfusion is also useful for evaluating patients who have cardiac and paracardiac pathologies, congenital and acquired heart diseases, and great vessel abnormalities because it requires a small amount of contrast agent and it can reveal the flow dynamics and morphology of the heart and great vessels when combined with cardiac MRI and CE-MRA.

Conflict of interest disclosure

The authors declared no conflicts of interest.

References

1. Balci NC, Yalçın Y, Tunacı A, Balcı Y. Assessment of the anomalous pulmonary circulation by dynamic contrast-enhanced MR angiography in under four seconds. Magn Reson Imaging 2003; 21:1–7.
2. Francois CJ, Shors SM, Bonow RO, Finn JP. Analysis of cardiopulmonary transit times at contrast material-enhanced MR imaging in patients with heart disease. Radiology 2003; 227:447–452.
3. Shors SM, Cotts WG, Pavlovic-Surjancev B, Francois CJ, Gheorghiade M, Finn JP. Heart failure: evaluation of cardiopulmonary transit times with time-resolved MR angiography. Radiology 2003; 229:743–748.
4. Tsai YH, Wu MT, Lin YR, et al. Temporal correlation-based dynamic contrast-enhanced MR imaging improves assessment of complex pulmonary circulation in congenital heart disease. Magn Reson Med 2006; 56:517–526.
5. de Bono D. Complications of diagnostic cardiac catheterization: results from 34,041 patients in the United Kingdom confidential enquiry into cardiac catheter complications. The Joint Audit Committee of the British Cardiac Society and Royal College of Physicians of London. Br Heart J 1993; 70:297–300.
6. Geva T, Greil GF, Marshall AC, Landzberg M, Powell AJ. Gadolinium-enhanced 3-dimensional magnetic resonance angiography of pulmonary blood supply in patients with complex pulmonary stenosis or atresia: comparison with x-ray angiography. Circulation 2002; 106:473–478.
7. Swan JS, Carroll TJ, Kennell TW, et al. Timeresolved three-dimensional contrast-enhanced MR angiography of the peripheral vessels. Radiology 2002; 225:43–52.
8. Prince MR. Gadolinium-enhanced MR aortography. Radiology 1994; 191:155–164.
9. Masui T, Katayama M, Kobayashi S, et al. Gadolinium-enhanced MR angiography in the evaluation of congenital cardiovascular disease pre-postoperative states in infants and children. J Magn Reson Imaging 2000; 12:1034–1042.
10. Holmqvist C, Larsson E-M, Stahlberg F, Laurin S. Contrast-enhanced thoracic 3D-MR angiography in infants and children. Acta Radiol 2001; 42:50–58.
11. Okuda S, Kikinis R, Geva T, Chung T, Dumanli H, Powell AJ. 3D-shaded surface rendering of gadolinium-enhanced MR angiography in congenital heart disease. Pediatr Radiol 2000; 30:540–545.
12. Ferrari VA, Scott CH, Holland GA, Axel L, Sutton MSJ. Ultrafast three-dimensional contrast enhanced magnetic resonance angiography and imaging in the diagnosis of partial anomalous venous drainage. J Am Coll Cardiol 2001; 37:1120–1128.
13. Haliloglu M, Hoffer FA, Gronemeyer SA, Rao BN. Applications of 3D contrast-enhanced MR angiography in pediatric oncology. Pediatr Radiol 1999; 29:863–868.
14. Goyen M, Laub G, Ladd ME, et al. Dynamic 3D MR angiography of the pulmonary arteries in under four seconds. J Magn Reson Imaging 2001; 13:372–377.
15. Goo HW, Yang DH, Park IS, et al. Time-resolved three-dimensional contrast-enhanced magnetic resonance angiography in patients who have undergone a Fontan operation or bidirectional cavopulmonary connection: Initial experience. J Magn Reson Imaging 2007; 25:727–736 .
16. Be'eri E, Maier SE, Landzberg MJ, Chung T, Geva T. In vivo evaluation of Fontan pathway flow dynamics by multidimensional phase-velocity magnetic resonance imaging. Circulation 1998; 98:2873–2882.
17. Fogel MA, Weingerg PM, Rychik J, et al. Caval contribution to flow in the branch pulmonary arteries of Fontan patients with a novel application of magnetic resonance presaturation pulse. Circulation 1999; 99:1215–1221.
18. Muthupillai R, Vick III GW, Flamm SD, Chung T. Time-resolved contrast-enhanced magnetic resonance angiography in pediatric patients using sensitivity encoding. J Magn Reson Imaging 2003; 17:559–564.
19. Chung T. Magnetic resonance angiography of the body in pediatric patients: experience with a contrast-enhanced time-resolved technique. Pediatr Radiol 2005; 35:3–1.
20. Sensky PR, Jivan A, Hudson NM, et al. Coronary artery disease: combined stress MR imaging protocol-one-stop evaluation of myocardial perfusion and function. Radiology 2000; 215:608–614.